

Search for the reaction channel $e^+e^- \rightarrow \eta_c\eta\pi^+\pi^-$ at center-of-mass energies from 4.23 to 4.60 GeV

M. Ablikim¹, M. N. Achasov^{10,d}, P. Adlarson⁵⁹, S. Ahmed¹⁵, M. Albrecht⁴, M. Alekseev^{58A,58C}, A. Amoroso^{58A,58C}, F. F. An¹, Q. An^{55,43}, Y. Bai⁴², O. Bakina²⁷, R. Baldini Ferroli^{23A}, I. Balossino^{24A}, Y. Ban^{35,l}, K. Begzsuren²⁵, J. V. Bennett⁵, N. Berger²⁶, M. Bertani^{23A}, D. Bettoni^{24A}, F. Bianchi^{58A,58C}, J. Biernat⁵⁹, J. Bloms⁵², I. Boyko²⁷, R. A. Briere⁵, H. Cai⁶⁰, X. Cai^{1,43}, A. Calcaterra^{23A}, G. F. Cao^{1,47}, N. Cao^{1,47}, S. A. Cetin^{46B}, J. Chai^{58C}, J. F. Chang^{1,43}, W. L. Chang^{1,47}, G. Chelkov^{27,b,c}, D. Y. Chen⁶, G. Chen¹, H. S. Chen^{1,47}, J. C. Chen¹, M. L. Chen^{1,43}, S. J. Chen³³, Y. B. Chen^{1,43}, W. Cheng^{58C}, G. Cibinetto^{24A}, F. Cossio^{58C}, X. F. Cui³⁴, H. L. Dai^{1,43}, J. P. Dai^{38,h}, X. C. Dai^{1,47}, A. Dbeysli¹⁵, D. Dedovich²⁷, Z. Y. Deng¹, A. Denig²⁶, I. Denysenko²⁷, M. Destefanis^{58A,58C}, F. De Mori^{58A,58C}, Y. Ding³¹, C. Dong³⁴, J. Dong^{1,43}, L. Y. Dong^{1,47}, M. Y. Dong^{1,43,47}, Z. L. Dou³³, S. X. Du⁶³, J. Z. Fan⁴⁵, J. Fang^{1,43}, S. S. Fang^{1,47}, Y. Fang¹, R. Farinelli^{24A,24B}, L. Fava^{58B,58C}, F. Feldbauer⁴, G. Felici^{23A}, C. Q. Feng^{55,43}, M. Fritsch⁴, C. D. Fu¹, Y. Fu¹, Q. Gao¹, X. L. Gao^{55,43}, Y. Gao⁴⁵, Y. Gao⁵⁶, Y. G. Gao⁶, Z. Gao^{55,43}, B. Garillon²⁶, I. Garzia^{24A}, E. M. Gersabeck⁵⁰, A. Gilman⁵¹, K. Goetzen¹¹, L. Gong³⁴, W. X. Gong^{1,43}, W. Gradl²⁶, M. Greco^{58A,58C}, L. M. Gu³³, M. H. Gu^{1,43}, S. Gu², Y. T. Gu¹³, A. Q. Guo²², L. B. Guo³², R. P. Guo³⁶, Y. P. Guo²⁶, A. Guskov²⁷, S. Han⁶⁰, X. Q. Hao¹⁶, F. A. Harris⁴⁸, K. L. He^{1,47}, F. H. Heinsius⁴, T. Held⁴, Y. K. Heng^{1,43,47}, M. Himmelreich^{11,g}, Y. R. Hou⁴⁷, Z. L. Hou¹, H. M. Hu^{1,47}, J. F. Hu^{38,h}, T. Hu^{1,43,47}, Y. Hu¹, G. S. Huang^{55,43}, J. S. Huang¹⁶, X. T. Huang³⁷, X. Z. Huang³³, N. Huesken⁵², T. Hussain⁵⁷, W. Ikegami Andersson⁵⁹, W. Imoehl²², M. Irshad^{55,43}, Q. Ji¹, Q. P. Ji¹⁶, X. B. Ji^{1,47}, X. L. Ji^{1,43}, H. L. Jiang³⁷, X. S. Jiang^{1,43,47}, X. Y. Jiang³⁴, J. B. Jiao³⁷, Z. Jiao¹⁸, D. P. Jin^{1,43,47}, S. Jin³³, Y. Jin⁴⁹, T. Johansson⁵⁹, N. Kalantar-Nayestanaki²⁹, X. S. Kang³¹, R. Kappert²⁹, M. Kavatsyuk²⁹, B. C. Ke¹, I. K. Keshk⁴, A. Khoukaz⁵², P. Kiese²⁶, R. Kiuchi¹, R. Kliemt¹¹, L. Koch²⁸, O. B. Kolcu^{46B,f}, B. Kopf⁴, M. Kuemmel⁴, M. Kuessner⁴, A. Kupsc⁵⁹, M. Kurth¹, M. G. Kurth^{1,47}, W. Kühn²⁸, J. S. Lange²⁸, P. Larin¹⁵, L. Lavezzi^{58C}, H. Leithoff²⁶, T. Lenz²⁶, C. Li⁵⁹, Cheng Li^{55,43}, D. M. Li⁶³, F. Li^{1,43}, F. Y. Li^{35,l}, G. Li¹, H. B. Li^{1,47}, H. J. Li^{9,j}, J. C. Li¹, J. W. Li⁴¹, Ke Li¹, L. K. Li¹, Lei Li³, P. L. Li^{55,43}, P. R. Li³⁰, Q. Y. Li³⁷, W. D. Li^{1,47}, W. G. Li¹, X. H. Li^{55,43}, X. L. Li³⁷, X. N. Li^{1,43}, Z. B. Li⁴⁴, Z. Y. Li⁴⁴, H. Liang^{1,47}, H. Liang^{55,43}, Y. F. Liang⁴⁰, Y. T. Liang²⁸, G. R. Liao¹², L. Z. Liao^{1,47}, J. Libby²¹, C. X. Lin⁴⁴, D. X. Lin¹⁵, Y. J. Lin¹³, B. Liu^{38,h}, B. J. Liu¹, C. X. Liu¹, D. Liu^{55,43}, D. R. Liu^{38,h}, F. H. Liu³⁹, Fang Liu¹, Feng Liu⁶, H. B. Liu¹³, H. M. Liu^{1,47}, Huanhuan Liu¹, Huihui Liu¹⁷, J. B. Liu^{55,43}, J. Y. Liu^{1,47}, K. Y. Liu³¹, Ke Liu⁶, L. Y. Liu¹³, Q. Liu⁴⁷, S. B. Liu^{55,43}, T. Liu^{1,47}, X. Liu³⁰, X. Y. Liu^{1,47}, Y. B. Liu³⁴, Z. A. Liu^{1,43,47}, Zhiqing Liu³⁷, Y. F. Long^{35,l}, X. C. Lou^{1,43,47}, H. J. Lu¹⁸, J. D. Lu^{1,47}, J. G. Lu^{1,43}, Y. Lu¹, Y. P. Lu^{1,43}, C. L. Luo³², M. X. Luo⁶², P. W. Luo⁴⁴, T. Luo^{9,j}, X. L. Luo^{1,43}, S. Lusso^{58C}, X. R. Lyu⁴⁷, F. C. Ma³¹, H. L. Ma¹, L. L. Ma³⁷, M. M. Ma^{1,47}, Q. M. Ma¹, X. N. Ma³⁴, X. X. Ma^{1,47}, X. Y. Ma^{1,43}, Y. M. Ma³⁷, F. E. Maas¹⁵, M. Maggiora^{58A,58C}, S. Maldaner²⁶, S. Malde⁵³, Q. A. Malik⁵⁷, A. Mangoni^{23B}, Y. J. Mao^{35,l}, Z. P. Mao¹, S. Marcello^{58A,58C}, Z. C. Meng⁴⁹, J. G. Messchendorp²⁹, G. Mezzadri^{24A}, J. Min^{1,43}, T. J. Min³³, R. E. Mitchell²², X. H. Mo^{1,43,47}, Y. J. Mo⁶, C. Morales Morales¹⁵, N. Yu. Muchnoi^{10,d}, H. Muramatsu⁵¹, A. Mustafa⁴, S. Nakhoul^{11,g}, Y. Nefedov²⁷, F. Nerling^{11,g}, I. B. Nikolaev^{10,d}, Z. Ning^{1,43}, S. Nisar^{8,k}, S. L. Niu^{1,43}, S. L. Olsen⁴⁷, Q. Ouyang^{1,43,47}, S. Pacetti^{23B}, Y. Pan^{55,43}, M. Papenbrock⁵⁹, P. Patteri^{23A}, M. Pelizaeus⁴, H. P. Peng^{55,43}, K. Peters^{11,g}, J. Pettersson⁵⁹, J. L. Ping³², R. G. Ping^{1,47}, A. Pitka⁴, R. Poling⁵¹, V. Prasad^{55,43}, H. R. Qi², M. Qi³³, T. Y. Qi², S. Qian^{1,43}, C. F. Qiao⁴⁷, N. Qin⁶⁰, X. P. Qin¹³, X. S. Qin⁴, Z. H. Qin^{1,43}, J. F. Qiu¹, S. Q. Qu³⁴, K. H. Rashid^{57,i}, K. Ravindran²¹, C. F. Redmer²⁶, M. Richter⁴, A. Rivetti^{58C}, V. Rodin²⁹, M. Rolo^{58C}, G. Rong^{1,47}, Ch. Rosner¹⁵, M. Rump⁵², A. Sarantsev^{27,e}, M. Savrié^{24B}, Y. Schelhaas²⁶, K. Schoenning⁵⁹, W. Shan¹⁹, X. Y. Shan^{55,43}, M. Shao^{55,43}, C. P. Shen², P. X. Shen³⁴, X. Y. Shen^{1,47}, H. Y. Sheng¹, X. Shi^{1,43}, X. D. Shi^{55,43}, J. J. Song³⁷, Q. Q. Song^{55,43}, X. Y. Song¹, S. Sosio^{58A,58C}, C. Sowa⁴, S. Spataro^{58A,58C}, F. F. Sui³⁷, G. X. Sun¹, J. F. Sun¹⁶, L. Sun⁶⁰, S. S. Sun^{1,47}, X. H. Sun¹, Y. J. Sun^{55,43}, Y. K. Sun^{55,43}, Y. Z. Sun¹, Z. J. Sun^{1,43}, Z. T. Sun¹, Y. T. Tan^{55,43}, C. J. Tang⁴⁰, G. Y. Tang¹, X. Tang¹, V. Thoren⁵⁹, B. Tsednee²⁵, I. Uman^{46D}, B. Wang¹, B. L. Wang⁴⁷, C. W. Wang³³, D. Y. Wang^{35,l}, K. Wang^{1,43}, L. L. Wang¹, L. S. Wang¹, M. Wang³⁷, M. Z. Wang^{35,l}, Meng Wang^{1,47}, P. L. Wang¹, R. M. Wang⁶¹, W. P. Wang^{55,43}, X. Wang^{35,l}, X. F. Wang¹, X. L. Wang^{9,j}, Y. Wang⁴⁴, Y. Wang^{55,43}, Y. F. Wang^{1,43,47}, Y. Q. Wang¹, Z. Wang^{1,43}, Z. G. Wang^{1,43}, Z. Y. Wang¹, Zongyuan Wang^{1,47}, T. Weber⁴, D. H. Wei¹², P. Weidenkaff²⁶, H. W. Wen³², S. P. Wen¹, U. Wiedner⁴, G. Wilkinson⁵³, M. Wolke⁵⁹, L. H. Wu¹, L. J. Wu^{1,47}, Z. Wu^{1,43}, L. Xia^{55,43}, Y. Xia²⁰, S. Y. Xiao¹, Y. J. Xiao^{1,47}, Z. J. Xiao³², Y. G. Xie^{1,43}, Y. H. Xie⁶, T. Y. Xing^{1,47}, X. A. Xiong^{1,47}, Q. L. Xiu^{1,43}, G. F. Xu¹, J. J. Xu³³, L. Xu¹, Q. J. Xu¹⁴, W. Xu^{1,47}, X. P. Xu⁴¹, F. Yan⁵⁶, L. Yan^{58A,58C}, W. B. Yan^{55,43}, W. C. Yan², Y. H. Yan²⁰, H. J. Yang^{38,h}, H. X. Yang¹, L. Yang⁶⁰, R. X. Yang^{55,43}, S. L. Yang^{1,47}, Y. H. Yang³³, Y. X. Yang¹², Yifan Yang^{1,47}, Z. Q. Yang²⁰, M. Ye^{1,43}, M. H. Ye⁷, J. H. Yin¹, Z. Y. You⁴⁴, B. X. Yu^{1,43,47}, C. X. Yu³⁴, J. S. Yu²⁰, T. Yu⁵⁶, C. Z. Yuan^{1,47}, X. Q. Yuan^{35,l}, Y. Yuan¹, A. Yuncu^{46B,a}, A. A. Zafar⁵⁷, Y. Zeng²⁰, B. X. Zhang¹, B. Y. Zhang^{1,43}, C. C. Zhang¹, D. H. Zhang¹, H. H. Zhang⁴⁴, H. Y. Zhang^{1,43}, J. Zhang^{1,47}, J. L. Zhang⁶¹, J. Q. Zhang⁴, J. W. Zhang^{1,43,47}, J. Y. Zhang¹, J. Z. Zhang^{1,47}, K. Zhang^{1,47}, L. Zhang⁴⁵, L. Zhang³³, S. F. Zhang³³, T. J. Zhang^{38,h}, X. Y. Zhang³⁷, Y. Zhang^{55,43}, Y. H. Zhang^{1,43}, Y. T. Zhang^{55,43}, Yang Zhang¹, Yao Zhang¹, Yi Zhang^{9,j}, Yu Zhang⁴⁷, Z. H. Zhang⁶, Z. P. Zhang⁵⁵, Z. Y. Zhang⁶⁰, G. Zhao¹, J. W. Zhao^{1,43}, J. Y. Zhao^{1,47}, J. Z. Zhao^{1,43}, Lei Zhao^{55,43}, Ling Zhao¹, M. G. Zhao³⁴, Q. Zhao¹, S. J. Zhao⁶³, T. C. Zhao¹, Y. B. Zhao^{1,43}, Z. G. Zhao^{55,43}, A. Zhemchugov^{27,b}, B. Zheng⁵⁶, J. P. Zheng^{1,43}, Y. Zheng^{35,l}, Y. H. Zheng⁴⁷, B. Zhong³², L. Zhou^{1,43}, L. P. Zhou^{1,47}, Q. Zhou^{1,47}, X. Zhou⁶⁰, X. K. Zhou⁴⁷, X. R. Zhou^{55,43}, Xiaoyu Zhou²⁰, Xu Zhou²⁰, A. N. Zhu^{1,47}, J. Zhu³⁴, J. Zhu⁴⁴, K. Zhu¹, K. J. Zhu^{1,43,47}, S. H. Zhu⁵⁴, W. J. Zhu³⁴, X. L. Zhu⁴⁵, Y. C. Zhu^{55,43}, Y. S. Zhu^{1,47}, Z. A. Zhu^{1,47}, J. Zhuang^{1,43}, B. S. Zou¹, J. H. Zou¹

(BESIII Collaboration)

¹ Institute of High Energy Physics, Beijing 100049, People's Republic of China² Beihang University, Beijing 100191, People's Republic of China³ Beijing Institute of Petrochemical Technology, Beijing 102617, People's Republic of China

- ⁴ Bochum Ruhr-University, D-44780 Bochum, Germany
- ⁵ Carnegie Mellon University, Pittsburgh, Pennsylvania 15213, USA
- ⁶ Central China Normal University, Wuhan 430079, People's Republic of China
- ⁷ China Center of Advanced Science and Technology, Beijing 100190, People's Republic of China
- ⁸ COMSATS University Islamabad, Lahore Campus, Defence Road, Off Raiwind Road, 54000 Lahore, Pakistan
- ⁹ Fudan University, Shanghai 200443, People's Republic of China
- ¹⁰ G.I. Budker Institute of Nuclear Physics SB RAS (BINP), Novosibirsk 630090, Russia
- ¹¹ GSI Helmholtzcentre for Heavy Ion Research GmbH, D-64291 Darmstadt, Germany
- ¹² Guangxi Normal University, Guilin 541004, People's Republic of China
- ¹³ Guangxi University, Nanning 530004, People's Republic of China
- ¹⁴ Hangzhou Normal University, Hangzhou 310036, People's Republic of China
- ¹⁵ Helmholtz Institute Mainz, Johann-Joachim-Becher-Weg 45, D-55099 Mainz, Germany
- ¹⁶ Henan Normal University, Xinxiang 453007, People's Republic of China
- ¹⁷ Henan University of Science and Technology, Luoyang 471003, People's Republic of China
- ¹⁸ Huangshan College, Huangshan 245000, People's Republic of China
- ¹⁹ Hunan Normal University, Changsha 410081, People's Republic of China
- ²⁰ Hunan University, Changsha 410082, People's Republic of China
- ²¹ Indian Institute of Technology Madras, Chennai 600036, India
- ²² Indiana University, Bloomington, Indiana 47405, USA
- ²³ (A)INFN Laboratori Nazionali di Frascati, I-00044, Frascati, Italy; (B)INFN and University of Perugia, I-06100, Perugia, Italy
- ²⁴ (A)INFN Sezione di Ferrara, I-44122, Ferrara, Italy; (B)University of Ferrara, I-44122, Ferrara, Italy
- ²⁵ Institute of Physics and Technology, Peace Ave. 54B, Ulaanbaatar 13330, Mongolia
- ²⁶ Johannes Gutenberg University of Mainz, Johann-Joachim-Becher-Weg 45, D-55099 Mainz, Germany
- ²⁷ Joint Institute for Nuclear Research, 141980 Dubna, Moscow region, Russia
- ²⁸ Justus-Liebig-Universitaet Giessen, II. Physikalisches Institut, Heinrich-Buff-Ring 16, D-35392 Giessen, Germany
- ²⁹ KVI-CART, University of Groningen, NL-9747 AA Groningen, The Netherlands
- ³⁰ Lanzhou University, Lanzhou 730000, People's Republic of China
- ³¹ Liaoning University, Shenyang 110036, People's Republic of China
- ³² Nanjing Normal University, Nanjing 210023, People's Republic of China
- ³³ Nanjing University, Nanjing 210093, People's Republic of China
- ³⁴ Nankai University, Tianjin 300071, People's Republic of China
- ³⁵ Peking University, Beijing 100871, People's Republic of China
- ³⁶ Shandong Normal University, Jinan 250014, People's Republic of China
- ³⁷ Shandong University, Jinan 250100, People's Republic of China
- ³⁸ Shanghai Jiao Tong University, Shanghai 200240, People's Republic of China
- ³⁹ Shanxi University, Taiyuan 030006, People's Republic of China
- ⁴⁰ Sichuan University, Chengdu 610064, People's Republic of China
- ⁴¹ Soochow University, Suzhou 215006, People's Republic of China
- ⁴² Southeast University, Nanjing 211100, People's Republic of China
- ⁴³ State Key Laboratory of Particle Detection and Electronics, Beijing 100049, Hefei 230026, People's Republic of China
- ⁴⁴ Sun Yat-Sen University, Guangzhou 510275, People's Republic of China
- ⁴⁵ Tsinghua University, Beijing 100084, People's Republic of China
- ⁴⁶ (A)Ankara University, 06100 Tandogan, Ankara, Turkey; (B)Istanbul Bilgi University, 34060 Eyup, Istanbul, Turkey; (C)Uludag University, 16059 Bursa, Turkey; (D)Near East University, Nicosia, North Cyprus, Mersin 10, Turkey
- ⁴⁷ University of Chinese Academy of Sciences, Beijing 100049, People's Republic of China
- ⁴⁸ University of Hawaii, Honolulu, Hawaii 96822, USA
- ⁴⁹ University of Jinan, Jinan 250022, People's Republic of China
- ⁵⁰ University of Manchester, Oxford Road, Manchester, M13 9PL, United Kingdom
- ⁵¹ University of Minnesota, Minneapolis, Minnesota 55455, USA
- ⁵² University of Muenster, Wilhelm-Klemm-Str. 9, 48149 Muenster, Germany
- ⁵³ University of Oxford, Keble Rd, Oxford, UK OX13RH
- ⁵⁴ University of Science and Technology Liaoning, Anshan 114051, People's Republic of China
- ⁵⁵ University of Science and Technology of China, Hefei 230026, People's Republic of China
- ⁵⁶ University of South China, Hengyang 421001, People's Republic of China
- ⁵⁷ University of the Punjab, Lahore-54590, Pakistan
- ⁵⁸ (A)University of Turin, I-10125, Turin, Italy; (B)University of Eastern Piedmont, I-15121, Alessandria, Italy; (C)INFN, I-10125, Turin, Italy
- ⁵⁹ Uppsala University, Box 516, SE-75120 Uppsala, Sweden
- ⁶⁰ Wuhan University, Wuhan 430072, People's Republic of China
- ⁶¹ Xinyang Normal University, Xinyang 464000, People's Republic of China
- ⁶² Zhejiang University, Hangzhou 310027, People's Republic of China
- ⁶³ Zhengzhou University, Zhengzhou 450001, People's Republic of China

^a Also at Bogazici University, 34342 Istanbul, Turkey

^b Also at the Moscow Institute of Physics and Technology, Moscow 141700, Russia

^c Also at the Functional Electronics Laboratory, Tomsk State University, Tomsk, 634050, Russia

^d Also at the Novosibirsk State University, Novosibirsk, 630090, Russia

^e Also at the NRC "Kurchatov Institute", PNPI, 188300, Gatchina, Russia

^f Also at Istanbul Arel University, 34295 Istanbul, Turkey

^g Also at Goethe University Frankfurt, 60323 Frankfurt am Main, Germany

^h Also at Key Laboratory for Particle Physics, Astrophysics and Cosmology, Ministry of Education; Shanghai Key Laboratory for Particle Physics and Cosmology; Institute of Nuclear and Particle Physics, Shanghai 200240, People's Republic of China

ⁱ Also at Government College Women University, Sialkot - 51310. Punjab, Pakistan.

^j Also at Key Laboratory of Nuclear Physics and Ion-beam Application (MOE) and Institute of Modern Physics, Fudan University, Shanghai 200443, People's Republic of China

^k Also at Harvard University, Department of Physics, Cambridge, MA, 02138, USA

^l Also at State Key Laboratory of Nuclear Physics and Technology, Peking University, Beijing 100871, People's Republic of China

Using data collected with the BESIII detector operating at the Beijing Electron Positron Collider, we search for the process $e^+e^- \rightarrow \eta_c \eta \pi^+ \pi^-$. The search is performed using five large data sets recorded at center-of-mass energies of 4.23, 4.26, 4.36, 4.42, and 4.60 GeV. The η_c meson is reconstructed in 16 exclusive decay modes. No signal is observed in the η_c mass region at any center-of-mass energy. The upper limits on the reaction cross sections are determined to be 6.2, 10.8, 27.6, 22.6 and 23.7 pb at the 90% confidence level at the center-of-mass energies listed above.

PACS numbers: 13.66 Bc, 13.66 Jn, 14.40 Lb, 14.40 Rt, 14.40 Pq

The BESIII collaboration has reported a charmonium like state $Z_c(3900)^\pm$ decaying into $J/\psi \pi^\pm$ in the reaction $e^+e^- \rightarrow J/\psi \pi^+ \pi^-$ at $\sqrt{s} = 4.26$ GeV [1]. This resonance was also observed by the Belle experiment [2] and confirmed using CLEO-c data [3]. In the CLEO-c dataset, evidence was found for the neutral state $Z_c(3900)^0$ in $e^+e^- \rightarrow J/\psi \pi^0 \pi^0$ [3], which was later also observed by BESIII [4]. The $Z_c(3900)$ can not be explained as a conventional meson, because of its decay to charmonia and the existence of its charged state.

An enhancement in the $D\bar{D}^*$ system at a mass of 3890.3 MeV/ c^2 has been observed in the reaction channel $e^+e^- \rightarrow \pi^+(D\bar{D}^*)^-$ at a center-of-mass energy of 4.26 GeV, which may be identified as the $Z_c(3900)^\pm$ [5]. Because of the observation of this second decay, interpretations favor the resonance to be either a tetra-quark state or a D -meson molecule [6]. In addition, a further charged resonance $Z_c(4020)^\pm$ was found in the subsystem $h_c \pi^\pm$ of the reaction $e^+e^- \rightarrow h_c \pi^+ \pi^-$, also at a center-of-mass energy of 4.26 GeV, closely followed by the discovery of its isospin partner the $Z_c(4020)^0$ [7, 8]. Furthermore, structures whose poles are compatible with the $Z_c(4020)$ have been observed by the BESIII collaboration in the reactions $e^+e^- \rightarrow \pi^+(D^* \bar{D}^*)^-$ and $e^+e^- \rightarrow \pi^0(D^* \bar{D}^*)^0$ [9, 10].

The observations of the isospin triplets $Z_c(3900)$ decaying to $J/\psi \pi$ and $Z_c(4020)$ decaying to $h_c \pi$ suggest the possibility of an unobserved triplet of $Z_c^{\pm,0}$ states decaying to $\eta_c \pi^{\pm,0}$ and an isospin-singlet state decaying to $\eta_c \eta$. Ref. [11] predicts a tetra-quark state in the mass region of 3.7 to 3.9 GeV with $J^{PC} = 0^{++}$ that would satisfy this latter hypothesis. The observation of this resonance would, therefore, add important information to the puzzle

of new states and would improve the understanding of their internal structure.

We search for the reaction $e^+e^- \rightarrow \eta_c \eta \pi^+ \pi^-$, as any events observed for this process will allow for studies of possible resonant structure in the $\eta_c \eta$ subsystem. The $\pi\pi$ system must have a relative angular momentum of $L=1$ to conserve C-parity. It is expected that this pion decay proceeds mainly via the ρ resonance (vector dominance model). This leads to suppression of the decay channel due to isospin conservation and, in addition, a limited phase space below center-of-mass energies of 4.3 GeV. Any observed events will also allow for studies of possible resonant substructures in the $\eta_c \pi^\pm$ subsystem.

A. Detector and Monte Carlo Simulation

The BESIII detector [12] is located at the BEPCII double-ring e^+e^- collider. The detector consists of a helium-based multi-layer drift chamber (MDC) with a momentum resolution of 0.5% for charged particles with a transverse momentum of 1 GeV/ c , a plastic scintillator based time-of-flight (TOF) system with a time resolution of 68 ps in the barrel and 110 ps in the end caps, a CsI(Tl) electromagnetic calorimeter (EMC) with energy resolutions of 2.5% and 5.0% for 1 GeV photons in the barrel and end caps respectively, and a multilayer resistive-plate chamber muon-detection system. The BESIII detector operates in a 1 T magnetic field provided by a superconducting solenoid and has a geometrical acceptance of 93%.

To optimize selection criteria, estimate detector resolution and reconstruction efficiency, Monte Carlo (MC) simulations are used. The simulation of the BESIII de-

detector is based on GEANT4 [13] which models the interaction of particles with the detector material. The initial interaction of the e^+e^- system is modeled with KKMC [14] generator which also handles initial state radiation. Subsequent particle decays are generated with EVTGEN [15]. The generation of final state radiation is handled by PHOTOS [16]. In the simulations the signal reaction channel $e^+e^- \rightarrow \eta_c \eta \pi^+ \pi^-$ is generated according to a phase-space distribution. The η_c is reconstructed in the following 16 decay modes: $\pi^+ \pi^- K^+ K^-$, $2(K^+ K^-)$, $2(\pi^+ \pi^-)$, $3(\pi^+ \pi^-)$, $K_S^0 K^\pm \pi^\mp$, $K_S^0 K^\pm \pi^\mp \pi^+ \pi^-$, $K^+ K^- \pi^0$, $K^+ K^- \eta$, $\pi^+ \pi^- \eta$, $\pi^+ \pi^- \pi^0 \pi^0$, $2(\pi^+ \pi^-) \eta$, $2(\pi^+ \pi^- \pi^0)$, $K^+ K^- 2(\pi^+ \pi^-)$, $p\bar{p}$, $p\bar{p}\pi^0$ and $p\bar{p}\pi^+ \pi^-$. The branching ratios for these decays are taken from Ref. [17]. The branching ratios of the decays $\pi^0 \rightarrow \gamma\gamma$, $\eta \rightarrow \gamma\gamma$, and $K_S^0 \rightarrow \pi^+ \pi^-$ are taken from the Particle Data Group (PDG) [18]. For the optimization of the suppression of background reactions various simulated data sets are used, e.g. samples containing light quark and open charm and charmonium final states as well as e^+e^- or $\mu^+\mu^-$ MC samples.

B. Data Analysis

The search for the reaction is performed at five different center-of-mass energies. The integrated luminosity of these data sets is given in Table I. During event reconstruction, the charged tracks are required to have a point of closest approach to the interaction point within a cylinder with a radius of $V_{xy} = 1$ cm in the x - y plane and a length of $V_z = \pm 10$ cm along the beam axis. In addition, the polar angle with respect to the beam axis has to be in the acceptance of the MDC, corresponding to $|\cos(\theta)| < 0.93$. For tracks originating from the decay of long lived particles like the K_S^0 meson, the V_{xy} requirement is omitted while V_z is increased to ± 20 cm. For each event, the net charge of all reconstructed tracks has to be zero. For particle identification, the joint probability from the energy loss in the MDC and the time-of-flight information of the TOF system is calculated for each particle species (π , K , p) and compared for the selection. Photons are reconstructed from clusters in the EMC. To suppress noise in the EMC, the reconstructed photon energy has to be larger than 25 MeV for $|\cos(\theta)| < 0.80$ and 50 MeV for $0.84 < |\cos(\theta)| < 0.92$. Furthermore, the time difference between the event-start time and the EMC timing information has to be $0 \text{ ns} \leq t_{\text{EMC}} \leq 700 \text{ ns}$. To suppress clusters formed by split-off photons from charged particle tracks, the angle between a cluster in the EMC and the closest charged track has to be at least 10° . The number of reconstructed photons has to be at least equal to the number of photons expected for the final state in question.

π^0 and η mesons are reconstructed from combinations of photon pairs. To select π^0 candidates, the invariant mass of two photons must satisfy $110 \text{ MeV}/c^2 \leq m_{\gamma\gamma} \leq 150 \text{ MeV}/c^2$ while for η candidates the invariant mass

has to be in range $500 \text{ MeV}/c^2 \leq m_{\gamma\gamma} \leq 570 \text{ MeV}/c^2$. Candidate K_S^0 mesons are reconstructed by applying a vertex fit to all pairs of oppositely charged particles assuming a pion hypothesis, but requiring no particle identification criteria. For these pairs the decay length L and its uncertainty σ_L are calculated from the decay vertex and the primary vertex position. The pair is kept as a K_S^0 candidate if the $\chi^2_{K_S^0}$ of the fit is smaller than 100. In addition, the decay length of the K_S^0 candidate has to satisfy $L/\sigma_L > 2$. Finally, the invariant mass of the pion pair must lie within 15 MeV/c^2 of the nominal K_S^0 mass.

A vertex fit is applied to events passing these criteria, excluding the tracks originating from K_S^0 candidates. In the cases that the vertex fit converges, a kinematic fit is performed to improve the momentum resolution. The fit is constrained by the initial four momentum of the e^+e^- pair and a mass constraint on the η mass. If the final state of the η_c contains additional π^0 , η or K_S^0 mesons, mass constraints are applied on the invariant masses of their daughter particles as well. The selection criteria on the χ^2 value from the kinematic fit is used to suppress poorly reconstructed events and is chosen for each final state to retain 90% of the signal events. The kinematic fit is not able to discriminate between pions from the initial reaction and pions from the subsequent η_c decay as the total four momentum is identical for these two hypotheses. This can lead to multiple candidates per event for the whole reconstruction, with each candidate having the same χ^2 . In these cases all candidates are kept for further analysis. It was checked with signal MC data sets that these candidates which have the wrong assignment do not contribute to the signal yield as the form a smooth background distribution. Also all other background distributions show a smooth behaviour at the signal region.

C. Cross Section and Upper-Limit Determination

To determine the total event yield of the reaction channel $e^+e^- \rightarrow \eta_c \eta \pi^+ \pi^-$ a simultaneous extended maximum-likelihood fit is performed on the invariant-mass distribution m of the η_c candidates for all η_c decay modes. The fit function f_{fit} is given by

$$f_{\text{fit}}(m | n_s, n_b, a_n) = n_s B(m | \mu_{\eta_c}^{\text{PDG}}, \Gamma_{\eta_c}^{\text{PDG}}) \otimes G(m | \mu, \sigma) + n_b \sum_{k=1}^n a_k T_k(m)$$

for each η_c decay mode separately. The signal shape for each decay mode is described by a Breit-Wigner function B , whose parameters are fixed to the nominal mass $\mu_{\eta_c}^{\text{PDG}}$ and width $\Gamma_{\eta_c}^{\text{PDG}}$ of the η_c meson from the PDG [18]. This function is convolved with a Gaussian function G with mean μ and standard deviation σ to account for the

TABLE I. Integrated luminosity of the used data samples and sum over all η_c final states of the products of the efficiencies and branching ratios at the different center-of-mass energies. The center-of-mass energies are taken from Ref. [19].

\sqrt{s} [MeV]	Luminosity [pb^{-1}]	$\sum_{X=1}^{16} \varepsilon_{tot,X} \mathcal{B}(\eta_c \rightarrow X)$ [%]
4225.54 ± 0.65	1091.7	2.07
4257.43 ± 0.66	825.7	2.10
4358.26 ± 0.62	539.8	2.23
4415.58 ± 0.64	1073.6	2.27
4599.53 ± 0.76	566.9	2.39

detector resolution, which is extracted from signal MC simulation. The number of background events (combinatorial and physical), n_b , for each η_c decay mode is determined simultaneously in the fit. For the majority of η_c decay modes the background is described by a n^{th} -order Chebychev polynomial function where the single terms T_k are weighted by the coefficients a_k . For certain decay modes ($\eta_c \rightarrow p\bar{p}$, $K^+K^-\eta$, $K^+K^-\pi^0$ and $K_sK\pi$) it is found that an exponential background function provides a better description of the background distribution. The number of signal events n_s in each η_c decay mode is related to the cross section σ via the relation

$$n_s = \varepsilon_{tot,X} \mathcal{B}(\eta_c \rightarrow X) \mathcal{B}(\eta \rightarrow \gamma\gamma) \mathcal{L} \sigma$$

where \mathcal{L} is the integrated luminosity, $\mathcal{B}(\eta_c \rightarrow X)$ the branching ratio of η_c decaying to X , and $\varepsilon_{tot,X}$ the corresponding reconstruction efficiency, which is obtained by fitting the reconstructed η_c invariant-mass distribution from signal MC simulation. Table I shows the sum over all η_c final states of the products of the efficiency and branching ratios. The invariant mass distribution summed over all decay modes is shown in Fig. 1 together with the sum of the fitting curves. The resulting values for the observed cross section can be found in Table II. The uncertainties are purely statistical and obtained by a likelihood scan using the MINOS tool [20].

As no significant signal is observed, an upper limit on the cross section is calculated. For this calculation a Bayesian approach is used. For the prior distribution $\pi(\sigma)$, we assume that it is zero for negative values of the cross section and follows a flat distribution otherwise. With this assumption the upper limit is given by

$$C(\sigma^{up}) = \frac{\int_{-\infty}^{\sigma^{up}} L(\sigma) \pi(\sigma) d\sigma}{\int_{-\infty}^{\infty} L(\sigma) \pi(\sigma) d\sigma} = \frac{\int_0^{\sigma^{up}} L(\sigma) d\sigma}{\int_0^{\infty} L(\sigma) d\sigma}.$$

where L is the likelihood function of the simultaneous fit as depicted in Fig. 2. The derived upper limits at 90% confidence level can also be found in Table II.

D. Systematic Uncertainties

There are several sources of possible systematic bias in the analysis, for which uncertainties are assigned. These

originate in discrepancies in the detector description between MC simulation and data, the knowledge of the η_c branching ratios, the knowledge of the resonance parameters of the η_c , the kinematic fit, and the background model and fit range used in the simultaneous fit. The systematic uncertainties are summarized in Table III.

The uncertainty associated with the understanding of the track reconstruction in the MDC is studied with the decays $J/\psi \rightarrow p\bar{p}\pi^+\pi^-$ and $J/\psi \rightarrow \rho\pi$ and is found to be 1% per charged track [21]. An additional 1% per track is applied to account for the knowledge of the particle identification performance [22]. The systematic uncertainty on the photon detection is estimated using the control samples $\psi(3680) \rightarrow \pi^+\pi^-J/\psi$ with $J/\psi \rightarrow \rho^0\pi^0$ and is determined to be smaller than 1% for each photon [23]. The systematic uncertainty on the K_S^0 reconstruction is estimated to be 1.2% using the control samples $J/\psi \rightarrow K^*(892)^\pm K^\mp$ with $K^*(892)^\pm \rightarrow K_s\pi^\pm$ and $J/\psi \rightarrow \phi K_s K^\pm \pi^\mp$ [24]. The systematic uncertainty associated with π^0 and η reconstruction is estimated to be 1% per π^0/η , following the studies reported in Ref. [25] using the control samples $J/\psi \rightarrow \pi^+\pi^-\pi^0$ and $J/\psi \rightarrow \eta p\bar{p}$. The influence of these uncertainties on the cross section extracted from the simultaneous fit is estimated by multiplying the reconstruction efficiency of each η_c final state X with a correction factor α_X , which is given by

$$\alpha_X = (\kappa_T)^{n_T} (\kappa_\gamma)^{n_\gamma} (\kappa_{\pi^0/\eta})^{n_{\pi^0/\eta}} (\kappa_{K_S^0})^{n_{K_S^0}}.$$

Each κ_Y (with $Y = T$ for tracks, γ for photons, π^0/η and K_S^0 for the reconstructed mesons) follows a Gaussian distribution centered at one and a width set to the corresponding uncertainty, while n_Y is the number of tracks, photons etc. in each final state X . The simultaneous fit is performed 1000 times while changing the values for κ_Y for each fit. The width of the resulting distribution normalized to the extracted cross-section is taken as the systematic uncertainty of the reconstruction efficiency.

The η_c branching ratios entering the simultaneous fit are derived from the BESIII measurement in Ref. [17], using the following relation

$$\mathcal{B}(\eta_c \rightarrow X) = \frac{\mathcal{B}(\psi(3680) \rightarrow \pi^0 h_c; h_c \rightarrow \gamma \eta_c; \eta_c \rightarrow X)}{\mathcal{B}(\psi(3680) \rightarrow \pi^0 h_c; h_c \rightarrow \gamma \eta_c)}.$$

Here the branching ratio $\mathcal{B}(\psi(3680) \rightarrow \pi^0 h_c; h_c \rightarrow \gamma \eta_c)$ is obtained by combining two measurements performed

TABLE II. Observed cross section σ and upper limits (UL) for the reaction $e^+e^- \rightarrow \eta_c\eta\pi^+\pi^-$ at the five center-of-mass energies. 3rd column: UL without systematic uncertainties, 4th column: UL with systematic uncertainties, 5th column: UL with systematic uncertainties plus ISR and vacuum polarization correction.

$E_{c.m.}$ [GeV]	σ [pb]	UL [pb]	UL with systematic uncertainties [pb]	UL after all correction [pb]
4.23	$-5.39^{+3.15}_{-2.83}$	3.5	4.2	6.2
4.26	$-0.98^{+4.11}_{-3.53}$	6.8	7.3	10.8
4.36	$8.59^{+6.72}_{-6.03}$	17.9	18.5	27.6
4.42	$3.07^{+5.36}_{-5.12}$	11.2	15.2	22.6
4.60	$3.16^{+6.91}_{-6.51}$	14.1	15.9	23.7

TABLE III. Total systematic uncertainty at the studied center-of-mass energies.

source	$\sigma_{\text{sys}}^{4.23 \text{ GeV}}$	$\sigma_{\text{sys}}^{4.26 \text{ GeV}}$	$\sigma_{\text{sys}}^{4.36 \text{ GeV}}$	$\sigma_{\text{sys}}^{4.42 \text{ GeV}}$	$\sigma_{\text{sys}}^{4.60 \text{ GeV}}$
Fit Range [pb]	0.23	0.57	0.79	0.51	0.05
Background Shape [pb]	1.53	1.43	0.48	5.59	3.97
η_c parameters [pb]	0.15	0.06	0.16	0.05	0.05
η_c branching ratio [%]	21.6	62.6	18.0	50.2	39.6
Reconstruction Efficiency [%]	12.8	23.5	11.3	12.0	13.8
Kinematic Fit [pb]	0.03	0.03	0.11	0.02	0.03
Luminosity [%]	1.0	1.0	1.0	1.0	1.0
total [pb]	2.05	1.67	2.04	5.83	4.19

by BESIII [26] and CLEO [27]. To estimate the systematic uncertainty of the branching ratios for the η_c final states a random number is drawn from a Gaussian distribution whose width is set to the total uncertainty of the combined measurement of the common denominator, and one for each of the 16 modes in the numerator separately. The simultaneous fit is performed again with the updated branching ratios. This is repeated 1000 times and the width of the obtained cross-section distribution normalized to the extracted cross-section is taken as systematic uncertainty.

During the simultaneous fit the mean and width of the signal Breit-Wigner distributions are fixed to the values given by the PDG [18]. To account for the uncertainties on these values, 1000 fits are performed in which new values for the mean and width of the η_c are randomly generated from two independent Gaussian probability distributions, with the parameters of these distributions set according to the central values and uncertainties of the PDG. The standard deviations of the resulting cross-section distributions are assigned as a systematic uncertainty in the measurement.

To improve the agreement of the χ^2 distribution of the kinematic fit between signal MC and data, the helix parameters of the charged tracks are smeared using the decay $J/\psi \rightarrow \phi f_0(980)$. The systematic uncertainty associated with the kinematic fit is estimated by switching off this correction, repeating the simultaneous fit and assigning the difference in the cross sections as the uncertainty.

The influence of the mass range over which the fit is performed is studied by narrowing and increasing the range of the fit by 5 MeV/ c^2 . The systematic uncertainty is calculated by taking the maximum difference of

the nominal fit value and the values obtained by varying the fit range.

The systematic uncertainty associated with the description of the background shape is estimated by increasing the order of the Chebychev polynomials by one. For those cases where the baseline description of the background is an exponential function, this is replaced by a second-order Chebychev polynomial. The difference between the cross section obtained with the new fit and that with the nominal background model is taken as the systematic uncertainty.

The integrated luminosity is determined by using Bhabha events. The systematic uncertainty of the luminosity measurement has been studied in Ref. [28] and a relative uncertainty of 1% is assigned for each center-of-mass energy.

To include the systematic uncertainties into the calculation of the upper limits, the likelihood is folded with a Gaussian distribution with a width set to the size of the systematic uncertainties

$$L_{\text{sys}}(\sigma) = \int_{-\infty}^{\infty} L(\sigma') \cdot G(\sigma'|\sigma, \sigma_{\text{sys}}) d\sigma'.$$

The likelihood graphs from this procedure are shown in Fig. 2. The upper limits for the observed cross sections including the systematic uncertainty are listed in Table II.

To obtain upper limits for the Born cross sections σ_{Born} , the observed cross sections have to be corrected for initial-state radiation (ISR) and vacuum polarization. The equation for the number of signal events in each η_c

decay mode then reads

$$n_s = \varepsilon_{X,tot} \mathcal{B}(\eta_c \rightarrow X) \mathcal{B}(\eta \rightarrow \gamma\gamma) \mathcal{L} \delta_{\text{ISR}} \delta_{vp} \sigma_{\text{Born}},$$

where $\varepsilon_{X,tot}$ is the total efficiency for final-state X , \mathcal{L} is the integrated luminosity, δ_{ISR} and δ_{vp} are the correction factors for initial-state radiation and vacuum polarization, respectively. The ISR correction factor is given by

$$\delta_{\text{ISR}} = \int \frac{\sigma(x) \varepsilon(x)}{\sigma_0 \varepsilon_0} W(x) dx.$$

Here x is the fraction of the beam energy carried away by the ISR photon, $\varepsilon(x)$ the corresponding reconstruction efficiency, $\sigma(x)$ is the line shape of a single resonance, which is assumed to have Breit-Wigner shape in the calculations, and σ_0 and ε_0 are their counterparts in the absence of initial-state radiation. $W(x)$ is the so-called radiator function [29]. The value of δ_{ISR} has a strong dependence on the parameters of the Breit-Wigner line shape, with the correction being largest for narrow resonances. As no resonances are observed, we make the conservative assumption that any resonance present has a width of 10 MeV/ c^2 which is well below the measured parameters of, for example, the Y(4260). For the determination of the upper limit the most conservative approach is taken by assuming this small resonance is located such that the correction factor is largest. The value of δ_{ISR} is estimated to be 0.64, independent of the collision energy and the η_c final state. This is shown in Table IV, together with the values of δ_{vp} , which are energy dependent and calculated with alphaQED [30]. The upper limits for the Born cross section are given in the right column of Table II.

$E_{c.m.}$ [GeV]	δ_{vp}	δ_{ISR}
4.23	1.056	0.64
4.26	1.054	0.64
4.36	1.051	0.64
4.42	1.053	0.64
4.60	1.055	0.64

TABLE IV. Values for the vacuum polarization and ISR corrections for the different data sets. Calculations of the vacuum polarization correction are based on alphaQED [30].

E. Summary and Results

We perform a search for the process $e^+e^- \rightarrow \eta_c \eta \pi^+ \pi^-$ at $\sqrt{s} = 4.23, 4.26, 4.36, 4.42$, and 4.60 GeV with data collected by the BESIII detector. The cross section at each center-of-mass energy is determined by a simultaneous fit to the invariant mass of the η_c meson for 16 decay

modes. The observed cross sections are determined to be

$$\begin{aligned} \sigma_{4.23 \text{ GeV}} &= -5.39_{-2.83}^{+3.15} \pm 2.05 \text{ pb} \\ \sigma_{4.26 \text{ GeV}} &= -0.98_{-3.53}^{+4.11} \pm 1.67 \text{ pb} \\ \sigma_{4.36 \text{ GeV}} &= 8.59_{-6.03}^{+6.72} \pm 2.04 \text{ pb} \\ \sigma_{4.42 \text{ GeV}} &= 3.07_{-5.12}^{+5.36} \pm 5.83 \text{ pb} \\ \sigma_{4.60 \text{ GeV}} &= 3.16_{-6.51}^{+6.91} \pm 4.19 \text{ pb}. \end{aligned}$$

where the first uncertainty is statistical, and the second systematic. As no significant signal is observed, upper limits on the Born cross sections are determined to be

$$\begin{aligned} \sigma_{4.23 \text{ GeV}}^{\text{up}} &= 6.2 \text{ pb} \\ \sigma_{4.26 \text{ GeV}}^{\text{up}} &= 10.8 \text{ pb} \\ \sigma_{4.36 \text{ GeV}}^{\text{up}} &= 27.6 \text{ pb} \\ \sigma_{4.42 \text{ GeV}}^{\text{up}} &= 22.6 \text{ pb} \\ \sigma_{4.60 \text{ GeV}}^{\text{up}} &= 23.7 \text{ pb} \end{aligned}$$

at the 90% confidence level. These upper limits are of the same order of magnitude as the measured cross sections of the processes $e^+e^- \rightarrow J/\psi \pi^+ \pi^-$ and $e^+e^- \rightarrow h_c \pi^+ \pi^-$ [7, 31]. As no significant $e^+e^- \rightarrow \eta_c \eta \pi^+ \pi^-$ signal is seen in the current data set it is not yet possible to conclude about possible resonant structures in the final-state subsystems.

Acknowledgments

The BESIII collaboration thanks the staff of BEPCII and the IHEP computing center for their strong support. This work is supported in part by National Key Basic Research Program of China under Contract No. 2015CB856700; National Natural Science Foundation of China (NSFC) under Contracts Nos. 11625523, 11635010, 11735014; National Natural Science Foundation of China (NSFC) under Contract No. 11835012; the Chinese Academy of Sciences (CAS) Large-Scale Scientific Facility Program; Joint Large-Scale Scientific Facility Funds of the NSFC and CAS under Contracts Nos. U1532257, U1532258, U1732263, U1832207; CAS Key Research Program of Frontier Sciences under Contracts Nos. QYZDJ-SSW-SLH003, QYZDJ-SSW-SLH040; 100 Talents Program of CAS; INPAC and Shanghai Key Laboratory for Particle Physics and Cosmology; German Research Foundation DFG under Contracts Nos. Collaborative Research Center CRC 1044, FOR 2359; Istituto Nazionale di Fisica Nucleare, Italy; Koninklijke Nederlandse Akademie van Wetenschappen (KNAW) under Contract No. 530-4CDP03; Ministry of Development of Turkey under Contract No. DPT2006K-120470; National Science and Technology fund; The Knut and Alice Wallenberg Foundation (Sweden) under Contract No. 2016.0157; The Royal Society, UK under Contract No. DH160214; The Swedish Research Council; U. S. Department of Energy under Contracts Nos. DE-FG02-

-
- [1] M. Ablikim *et al.* (BESIII Collaboration), *Phys. Rev. Lett.* **110**, 252001 (2013).
- [2] Z. Q. Liu *et al.* (Belle Collaboration), *Phys. Rev. Lett.* **110**, 252002 (2013).
- [3] T. Xiao *et al.*, *Phys. Lett. B* **727**, 366 (2013).
- [4] M. Ablikim *et al.* (BESIII Collaboration), *Phys. Rev. Lett.* **115**, 112003 (2015).
- [5] M. Ablikim *et al.* (BESIII Collaboration), *Phys. Rev. Lett.* **112**, 022001 (2014).
- [6] Q. Wang *et al.*, *Phys. Rev. Lett.* **111**, 132003 (2013).
- [7] M. Ablikim *et al.* (BESIII Collaboration), *Phys. Rev. Lett.* **111**, 242001 (2013).
- [8] M. Ablikim *et al.* (BESIII Collaboration), *Phys. Rev. Lett.* **113**, 212002 (2014).
- [9] M. Ablikim *et al.* (BESIII Collaboration), *Phys. Rev. Lett.* **112**, 132001 (2014).
- [10] M. Ablikim *et al.* (BESIII Collaboration), *Phys. Rev. Lett.* **115**, 182002 (2015).
- [11] N. Drenska *et al.*, *Riv. Nuovo Cim.* **33**, 633 (2010).
- [12] M. Ablikim *et al.* (BESIII Collaboration), *Nucl. Instrum. Meth. A* **614**, 345 (2010).
- [13] S. Agostinelli *et al.* (GEANT4 Collaboration), *Nucl. Instrum. Meth. A* **506**, 250 (2003).
- [14] S. Jadach *et al.*, *Phys. Rev. D* **63**, 113009 (2001).
- [15] R. G. Ping, *Chin. Phys. C* **32**, 599 (2008).
- [16] B. v. E. E. Barberio and Z. Was, *Comput. Phys. Commun.* **66**, 115 (1991).
- [17] M. Ablikim *et al.* (BESIII Collaboration), *Phys. Rev. D* **86**, 092009 (2012).
- [18] C. Patrignani *et al.* (Particle Data Group), *Chin. Phys. C* **40**, 100001 (2016).
- [19] M. Ablikim *et al.* (BESIII Collaboration), *Chin. Phys. C* **40**, 063001 (2015).
- [20] W. Eadie *et al.*, *Statistical Methods in Experimental Physics* (North-Holland Publ. Co., 1971).
- [21] M. Ablikim *et al.* (BESIII Collaboration), *Phys. Rev. Lett.* **112**, 251801 (2014).
- [22] M. Ablikim *et al.* (BESIII Collaboration), *Phys. Rev. D* **100**, 012003 (2019).
- [23] M. Ablikim *et al.* (BESIII Collaboration), *Phys. Rev. D* **83**, 112005 (2011).
- [24] M. Ablikim *et al.* (BESIII Collaboration), *Phys. Rev. D* **92**, 112008 (2015).
- [25] M. Ablikim *et al.* (BESIII Collaboration), *Phys. Rev. D* **81**, 052005 (2010).
- [26] M. Ablikim *et al.* (BESIII Collaboration), *Phys. Rev. Lett.* **104**, 132002 (2010).
- [27] S. Dobbs *et al.* (CLEO Collaboration), *Phys. Rev. Lett.* **101**, 182003 (2008).
- [28] M. Ablikim *et al.* (BESIII Collaboration), *Chin. Phys. C* **39**, 093001 (2015).
- [29] R. G. Ping *et al.*, *Chin. Phys. C* **38**, 083011 (2014).
- [30] F. Jegerlehner, *Nuovo Cim. C* **34**, 31 (2011).
- [31] M. Ablikim *et al.* (BESIII Collaboration), *Phys. Rev. Lett.* **118**, 092001 (2017).

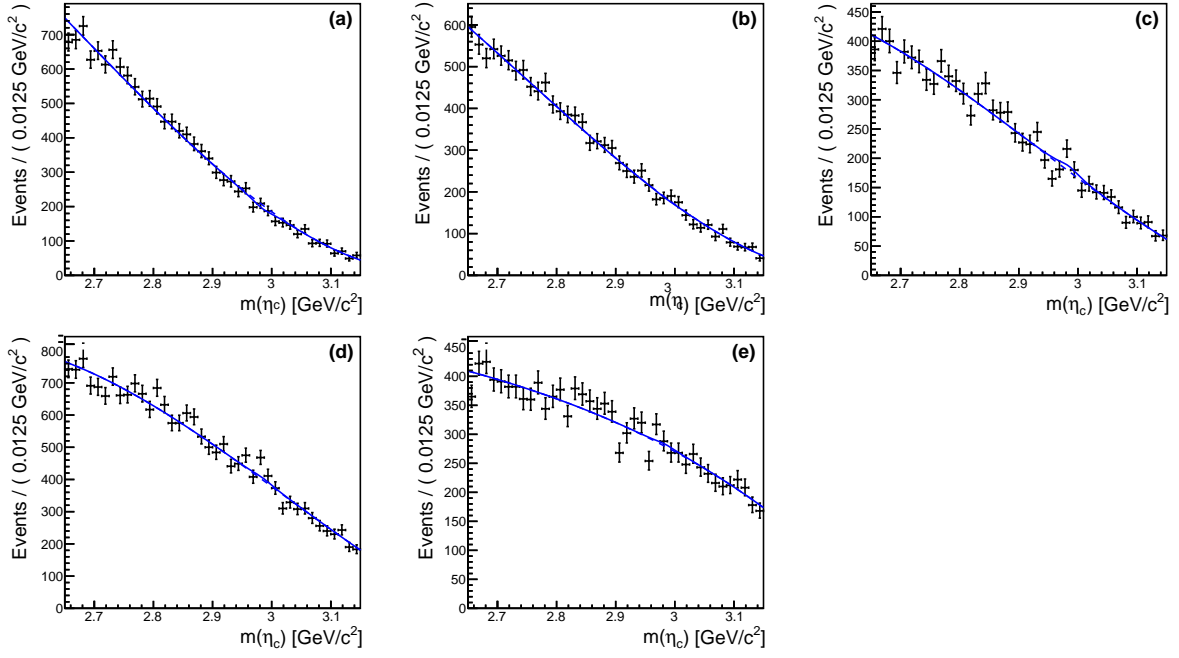


FIG. 1. Result of the simultaneous fit to 16 η_c decay modes. Shown is the sum of all modes at \sqrt{s} of 4.23 GeV (a), 4.26 GeV (b), 4.36 GeV (c), 4.42 GeV (d), and 4.60 GeV (e). Black points are data, blue line is the sum of the fitting functions.

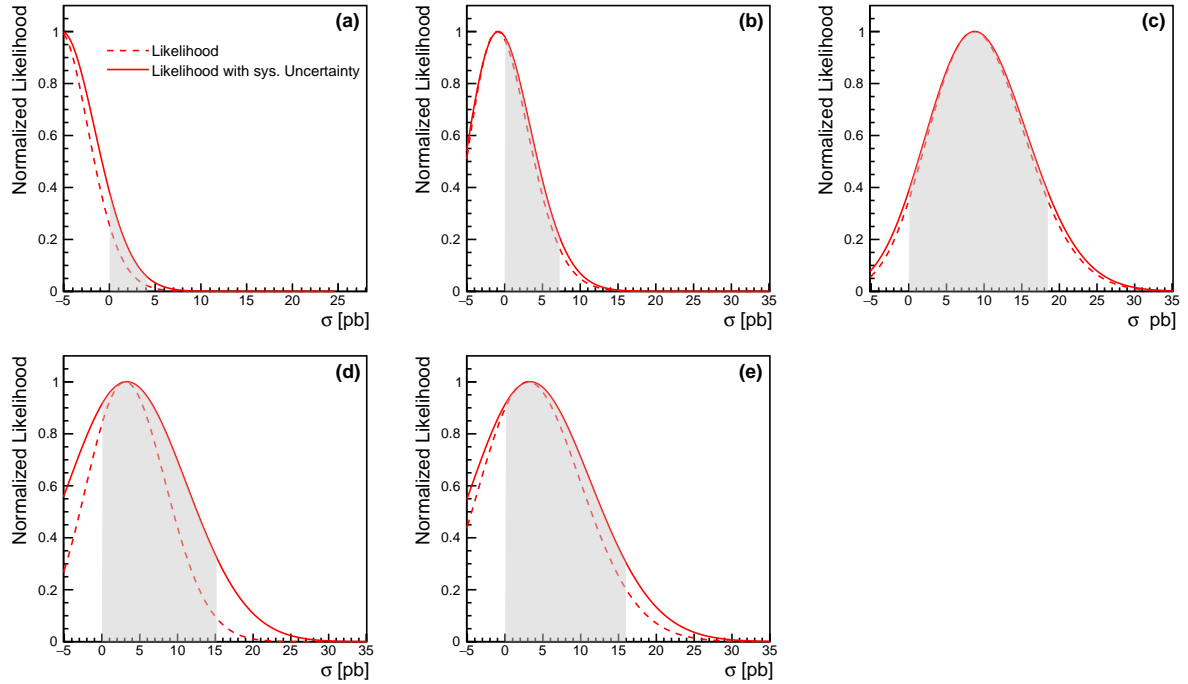


FIG. 2. Likelihood curves convoluted with the Gaussian function representing the systematic uncertainties as a function of the cross section at \sqrt{s} of 4.23 GeV (a), 4.26 GeV (b), 4.36 GeV (c), 4.42 GeV (d), and 4.60 GeV (e). The interval corresponding to the upper limit at 90% confidence level is indicated as gray area.